Eur. Phys. J. A **21**, 169–174 (2004)
DOI 10.1140/epja/i2003-10191-2

THE EUROPEAN PHYSICAL JOURNAL A

Fast-electron ejection from C, Ni, Ag and Au foils by $^{36}Ar^{18+}$ (95 MeV/u): Measurements of absolute cross-sections

E. De Filippo[1,a], G. Lanzanò[1], H. Rothard[2], C. Volant[3], S. Aiello[1], A. Anzalone[4], N. Arena[1], M. Geraci[1], F. Giustolisi[4], and A. Pagano[1]

[1] INFN and Dipartimento di Fisica e Astronomia, Via S. Sofia 64, I-95123 Catania, Italy
[2] Centre Interdisciplinaire de Recherche Ions Lasers (CEA/CNRS UMR 6637/ENSICAEN), CIRIL-Ganil, BP 5133, F-14070 Caen Cedex 05, France
[3] DAPNIA/SPhN, CEA/Saclay, F-91191 Gif-sur-Yvette Cedex, France
[4] INFN-LNS and Dipartimento di Fisica e Astronomia, Via S. Sofia 44, I-95123 Catania, Italy

Received: 1 July 2003 / Revised version: 15 December 2003 /
Published online: 13 July 2004 –
Communicated by D. Schwalm

Abstract. Doubly differential electron velocity spectra induced by $^{36}Ar^{18+}$ (95 MeV/u) from thin target foils (C, Ni, Ag, Au) were measured at GANIL (Caen, France) by means of the ARGOS multidetector and the time-of-flight technique. The main features observed in the forward spectra are convoy electrons, binary-encounter electrons, and (for the Au target only) a high-velocity tail which we attribute to a "Fermi shuttle" acceleration mechanism. Backward spectra do not show distinct structures. The spectra allow us to determine absolute singly differential cross-sections as a function of the target material and the emission angle. The convoy electron yield increases with the target atomic number, but for C their yield is so small that our experiment is not able to detect them. Absolute doubly differential cross-sections for binary-encounter electron ejection from C targets are well described by a transport theory which is based on the relativistic electron impact approximation (EIA) for electron production and which accounts for angular deflection, energy loss and energy straggling of the transmitted electrons.

PACS. 34.50.Fa Electronic excitation and ionization of atoms (including beam-foil excitation and ionization) – 79.20.Rf Atomic, molecular, and ion beam impact and interactions with surfaces – 25.70.-z Low and intermediate energy heavy-ion reactions

1 Introduction

Swift heavy-ion–induced effects in condensed matter have important applications in, *e.g.*, materials science (nanostructuring) and radiation medicine (hadron therapy for cancer treatment). In this respect, in recent years, beams of argon ions at the highest energies which can be obtained at GANIL (95 MeV/u) were widely used for research in radiation chemistry (radiolysis) and radiation biology [1]. The first step of radiation effects at high energies, where projectile-target electron collisions are the dominant process of energy loss, is electron ejection from target atoms. The primary electrons and their subsequent secondary interactions lead to the deposition of energy around the ion trajectory. The detailed knowledge of the structure of these ion tracks is a key issue for our understanding of radiation effects in condensed matter, an important example being calculations of the RBE (relative biological efficiency) of heavy particles, where doubly differential cross-sections (DDCS) for electron ejection are a key input parameter. Usually, data obtained from single collisions, *i.e.* with gas targets, are used, but condensed-matter effects may considerably alter the emission patterns. Also in nuclear-physics experiments concerning heavy-ion collisions at intermediate energies (20 MeV/u to 200 MeV/u), where most often thin solid foils are used as targets, energetic electrons disturb particle detectors, especially those working with low detection threshold. Thus, a detailed knowledge of electron angular and velocity distributions is very useful. Therefore, we measured DDCS for fast-electron ejection by $^{36}Ar^{18+}$ (95 MeV/u) from thin solid foils (C, Ni, Ag, Au).

In the forward direction (*i.e.* at the exit side, where the ion beam leaves the target foil), fast electrons are essentially produced by two reaction mechanisms. A binary encounter (BE) between the incident ion and an atomic

[a] e-mail: defilippo@ct.infn.it

electron produces electrons with a maximum velocity of about twice the projectile velocity v_P [2]. Since electrons are bound to the target nucleus in different shells, the observed distribution of BE electrons at fixed angle reflects the initial momentum distribution of the bound electrons of the target ("Compton profile"). Also, target electrons may be captured or projectile electrons may be lost into low-lying projectile centered continuum states. These so-called convoy electrons [3] travel with a velocity close to the projectile velocity and lead to a cusp-shaped peak in electron spectra.

Ejection of binary electrons from solids at high beam energies (above 10 MeV/u) was studied experimentally in the velocity range 13 MeV/u to 400 MeV/u [4–12]. Earlier studies used magnetic momentum analyzers and channeltrons or solid-state detectors for particle counting. The more recent studies performed with the ARGOS multidetector, based on time-of-flight techniques and scintillators, at LNS/Catania and GANIL/Caen, allowed the measurements of absolute cross-sections [11,12].

As far as the mathematical description is concerned, a relativistic version of the electron impact approximation (EIA) has been developed by Jakubaßa-Amundsen [12]. The ejection of BE electrons from the target by heavy, highly charged projectiles in a single collision is treated as quasi-elastic scattering, where ionization takes place via electron transfer to the projectile continuum. The corresponding cross-section is then folded with the electron momentum distribution (Compton profile) in its initial state. The transport of fast BE electrons traveling through the solid towards the surface was recently included in the theoretical treatment (S-EIA) [9,11]. A careful comparison between experimental results for doubly differential cross-section for binary-encounter electron ejection from C targets (induced by 95 MeV/u Ar^{18+}) and theory was recently performed in ref. [13].

2 Experimental method

The experiments were performed at GANIL in Caen/France. We used the following targets: ^{12}C of 100 $\mu g/cm^2$ and 1025 $\mu g/cm^2$ thickness, ^{58}Ni of 570 $\mu g/cm^2$, ^{nat}Ag of 560 $\mu g/cm^2$, ^{197}Au targets of 130 $\mu g/cm^2$ and 490 $\mu g/cm^2$. The pulsed 95 MeV/u $^{36}Ar^{18+}$ beam had a pulse width of about 500 ps. The multidetector ARGOS, consisting in about 100 scintillation detectors (so-called "phoswiches") was mounted inside the big scattering chamber NAUTILUS of GANIL for a complete detection and identification of electrons and nuclear-reaction products [6,8]. Electrons were detected in a large angular range from 3° to 173°. Particles (and in particular, electrons) were identified by shape discrimination of the photomultiplier signals (the "fast" and "slow" components of the detector), and their velocity was determined by measuring their times of flight as described in detail in [6].

An absolute velocity calibration was obtained from the prompt γ-ray peak due to nuclear reactions in the target, from elastically scattered projectiles, and from target X-rays. At electron velocities below $\approx$ 7.5 cm/ns (corresponding to an electron energy of $\approx$ 20 keV), detection threshold effects occur, *i.e.* the detection efficiency decreases. This affects the low-velocity part of the spectra as described in [6,8,10]. It is important to note that, due to the higher beam energy, threshold effects are less important here than in our previous experiments at lower projectile velocity. This is in particular true for the convoy electron peak. The energy of convoy electrons is $\approx$ 25 and $\approx$ 50 keV with 45 and 95 MeV/u beams, respectively, to be compared to the threshold of $\approx$ 20 keV. Therefore, the complete convoy electron velocity spectrum could be measured at the most forward angles in the present experiment.

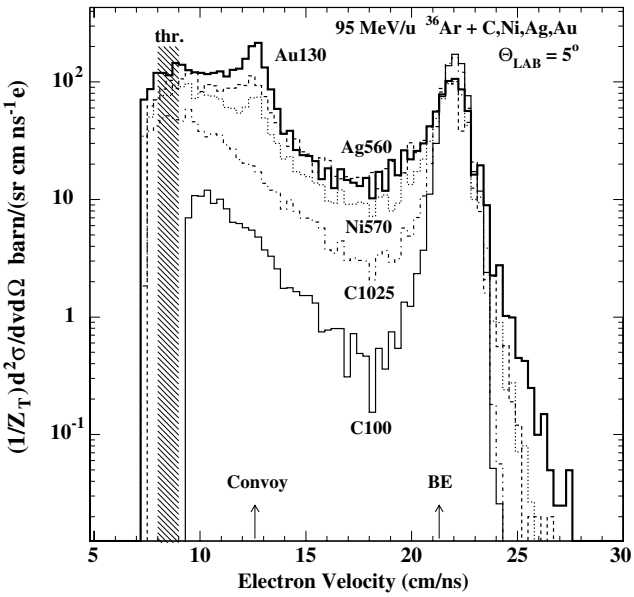

Fig. 1. Absolute forward electron velocity spectra for the reaction $^{36}Ar^{18+}$ (95 MeV/u) + C, Ni, Ag, Au at a laboratory angle of 5° (target thickness as indicated, in $\mu g/cm^2$). The binary-encounter (BE) and convoy electron components of the spectra are depicted by arrows. The shadowed area indicates the electronic threshold. Note the absence of the convoy component in the case of the carbon target. The absolute cross-sections are divided by the target atomic number Z_T.

Absolute cross-sections can be calculated from the number of incoming projectiles (measured with a Faraday cup) and from the number of electrons detected in the scintillation detectors (their detection efficiency being equal to unity for high-energy electrons). Thus, the detector solid angle can be calculated in a straightforward way from geometrical considerations only, *i.e.* from the detector area and the distance between target and detector (typically about 0.6 meters to 5.3 meters).

3 Results: target material dependence of electron emission

Velocity spectra of electrons from the impact of a 95 MeV/u $^{36}Ar^{18+}$ beam on different targets (C, Ni, Ag,

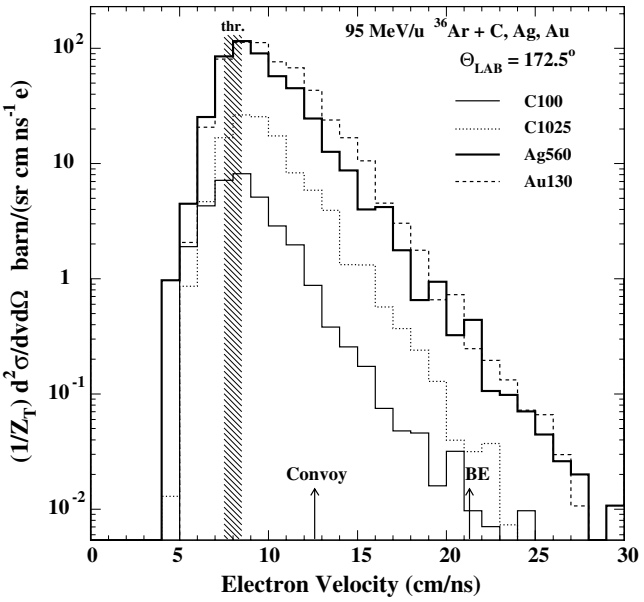

Fig. 2. Absolute backward electron velocity spectra for the reaction $^{36}Ar^{18+}$ (95 MeV/u) + C, Ag, Au at a laboratory angle of 172.5° (target thickness as indicated, in $\mu g/cm^2$). The shadowed area indicates the electronic threshold.

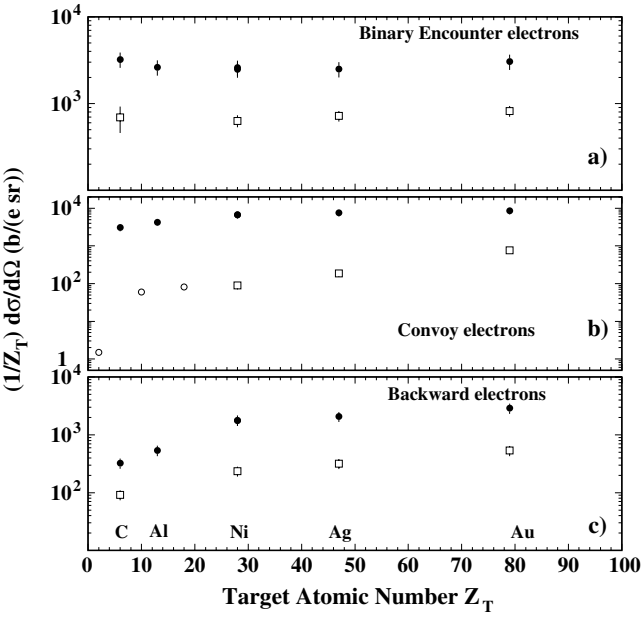

Fig. 3. Velocity-integrated absolute singly differential electron ejection cross-sections SDCS, induced by $^{36}Ar^{18+}$ (95 MeV/u) impact on C, Ni, Ag and Au (empty squares) as a function of the target atomic number Z_T: a) for binary-encounter electrons at 5° ejection angle, b) for the convoy electron component at 5°, c) for backward electrons at 130° ($v_e \geq 7.5$ cm/ns). Data for $^{58}Ni^{28+}$ (45 MeV/u) projectiles on C, Al, Ni, Ag and Au from a previous experiment at LNS Catania [10] at slightly different ejection angles of 6° (BE, CE) and 140° (backward electrons) are also shown (full circles). Note that the absolute production cross-section is not only given per atom, but per electron, *i.e.* it was divided by the target atomic number Z_T. The ECC (electron capture to continuum yields, empty circles) for bare Ar of 8.5 MeV/u at 0° on He, Ne and Ar are taken from [3] and scaled to our Ar data at 5° (see text).

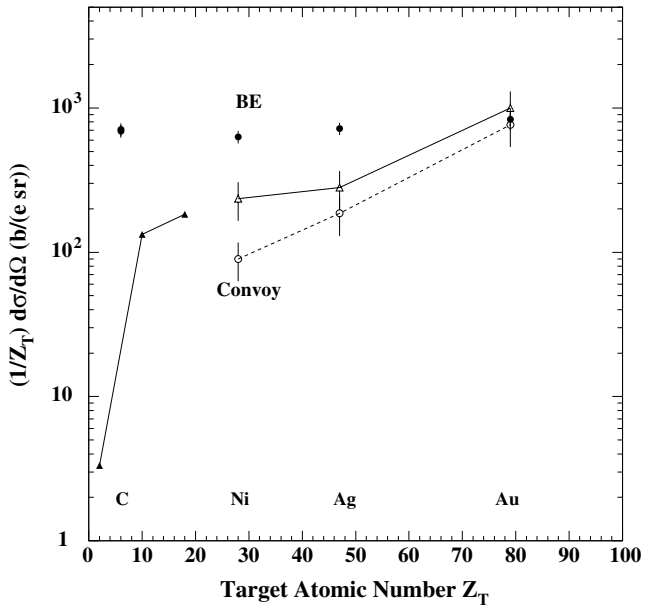

Fig. 4. Velocity-integrated absolute single differential electron ejection cross-sections SDCS, induced by $^{36}Ar^{18+}$ (95 MeV/u) impact on C, Ni, Ag and Au as a function of the target atomic number: full circles: binary-encounter electrons at 5° ejection angle, open circles: convoy electron component at 5°, open triangles: convoy electron component at 2°, full triangles: ECC (electron capture to continuum yields) for bare Ar of 8.5 MeV/u from Breinig *et al.* [3], normalized to our Ar data at 2°. Lines are drawn to guide the eye.

Au) are shown in fig. 1 (forward direction, beam exit side of the foils at 5°) and fig. 2 (backward direction, beam entrance side, at 172.5°). In the forward spectra of fig. 1, as main features, we observe two distinct, well-known components: fast binary-encounter (BE) electrons at almost twice the projectile velocity, and electrons with a velocity close to the beam velocity, the so-called convoy electrons (CE). The backward spectra of fig. 2 are without distinct structures, but show a strong target dependence.

Figures 3, 4 and 5 show velocity-integrated absolute values (*i.e.*, singly differential cross-sections). In fig. 3a and b, the BE and CE components, respectively, from fig. 1 are shown as a function of the target atomic number Z_T, for the 95 MeV/u $^{36}Ar^{18+}$ beam (empty squares). We also included data from a previous experiment performed at LNS Catania with 45 MeV/u $^{58}Ni^{28+}$ (full circles) [10]. In all cases, the yields, *i.e.* the singly differential cross-sections (SDCS), are obtained from Gaussian fits to the peaks as described in [8]. Data for ECC (electron capture to continuum, empty circles) yields for bare Ar of 8.5 MeV/u at 0° on He, Ne and Ar taken from [3] are also plotted in fig. 3b. These ECC yields were reported in arbitrary units and are scaled so that a smooth continuation with respect to our absolute data as a function of Z_T is obtained.

In fig. 3c, we show the backward yields from fig. 2 at 130° for Ar projectiles, and also yields of electrons emitted at 140° for Ni projectiles. The experimental points

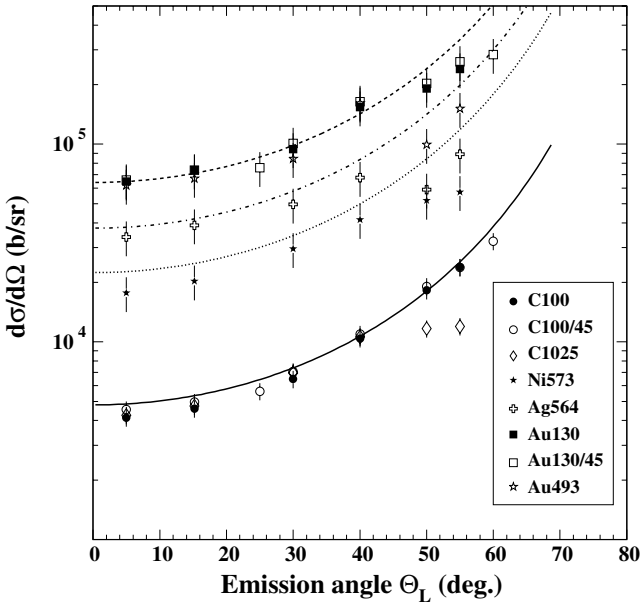

Fig. 5. Velocity-integrated absolute SDCS for BE electron emission as a function of the laboratory ejection angle θ for the reaction $^{36}Ar^{18+}$ (95 MeV/u) + C, Ni, Ag, Au as indicated in the figure. The solid line represents the theoretical calculation (EIA) for carbon, the dashed (Au), dash-dotted (Ag) and dotted (Ni) lines represent a simple scaling of the theory with SDCS(Z_T) = SDCS($Z_T = 6$) × $Z_T/6$ for $Z_T = 28$, 47, 79. Transport effects are not taken into account. Target thickness as indicated, in μg/cm^2. Data with targets tilted at 45° are also noted.

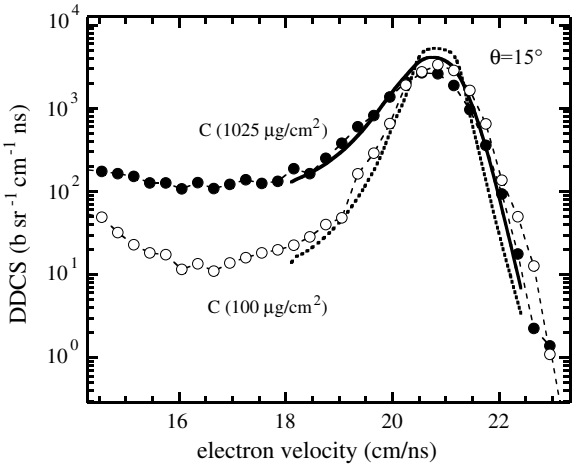

Fig. 6. Absolute doubly differential electron ejection cross-sections (DDCS) for carbon targets after $^{36}Ar^{18+}$ (95 MeV/u) impact at a laboratory angle of 15°. Experimental data (dashed lines are drawn to guide the eye): thick carbon target of 1025 μg/cm^2 (full circles), thin carbon target of 100 μg/cm^2 (open circles). Theory (relativistic transport theory S-EIA): thick carbon target of 1025 μg/cm^2 (solid line), thin carbon target of 100 μg/cm^2 (dotted line).

have been obtained by integrating the electron velocity spectra starting from a velocity of ≈ 7.5 cm/ns (below this velocity, detection threshold effects occur), up to the high-velocity part of the spectrum, which extends up to two times the beam velocity.

Figure 4 shows the BE yields (full circles) and the convoy yields at two different ejection angles (5°, open circles, and 2°, open triangles). Again, comparison is made to the ECC yields from Breinig *et al.* [3] (with a slightly different scaling of the arbitrary ECC yields as in fig. 3b). The angular distribution of BE, *i.e.* the SDCS as a function of the emission angle θ, is shown in fig. 5 for the different targets.

4 Discussion

4.1 Binary-encounter electrons

As a function of the target atomic number Z_T, the BE production cross-section (scaled per number of electrons of the target atom) is almost constant within error bars. This means that the BE intensities are roughly, but in a good approximation, proportional to the number of electrons "seen" by the projectile on its way through the target, since the intensities are normalized to the number of electrons per unit area [7].

The angular distribution of BE (SDCS from velocity integration of DDCS) as a function of the emission angle θ and the theoretical calculation (EIA) for carbon [9,12] is shown in fig. 5. Also shown is a simple scaling of the theory with SDCS(Z_T) = SDCS($Z_T = 6$) × $Z_T/6$. Transport effects are not taken into account in these calculations. Within error bars, the data points for the carbon target fall exactly on the theoretical curve. Also for the gold target at emission angles up to 40° the scaling is excellent. For the other targets, although the absolute values fall slightly below the theory, the angular dependence follows the theoretical curves, which are in fact close to a $1/\cos^3\theta_L$ law up to angles of about $\theta = 50°$. At larger angles, stronger deviations occur between data and calculations, and this is the case also for the gold and the thickest carbon target. They are probably due to peak broadening by electron transport effects which could also cause difficulties for correct background subtraction, and possibly also due to threshold effects, since the BE energy decreases with emission angle. The simple scaling law of a proportional relation to Z_T, *i.e.* to the number of "seen" target electrons, works quite well, as we have already seen above (fig. 3a).

Let us now compare measured absolute DDCS for carbon targets (emission angle $\theta = 15°$) to the calculated DDCS in fig. 6. The experimental resolution is approximately $\Delta p/p = 0.08$, and the theory is averaged according to this experimental resolution. The experimental results are represented by circles, the calculations, based on the relativistic transport theory [9,11], by lines. The peak shape is well reproduced by theory. The absolute value of the measured DDCS is slightly overpredicted by theory, but the overall agreement of the absolute values is remarkable. Notice, however that for the thinnest target,

the theory has a tendency to predict a too narrow width of the peak [13].

4.2 Convoy electrons

For completely stripped projectiles and atomic targets, convoy electrons are essentially produced by "electron capture to the projectile continuum" (ECC) [3]. With solid targets, also a multistep process, *i.e.* capture to bound projectile states followed by subsequent "electron loss to continuum" (ELC) [3] was considered and referred to as "indirect electron loss to the continuum" (IELC) [14].

As can be seen from fig. 3b, the production cross-section shows a strong dependence on the target atomic number. The evolution of the CE production cross-section as a function of the target atomic number is very similar at 45 MeV/u and at 95 MeV/u, and closely resembles the evolution of the ECC data of the Oak Ridge group obtained with bare Ar projectiles at 8.5 MeV/u [3], which we also show in fig. 3b.

From fig. 4 we clearly see that the CE yield depends on the ejection angle, it is higher at 2° than at 5°, because the convoy electron velocity distribution is peaked around 0°. Absolute values are much smaller for Ar projectiles than for Ni because of the higher velocity and lower projectile nuclear charge. The ECC cross-section strongly depends on v_P and Z_T. Under charge equilibrium conditions, convoy electron yields were found to depend weakly on the target atomic number (the convoy electron yield is about a factor of 2 higher with Au targets than with C targets), but strongly on projectile charge and velocity. The yields scale with the projectile nuclear charge as $Z_P^{2.75}$, and decrease at least as strongly as $v_P^{-4.5}$ with projectile velocity [3,14]. An estimate from this empirical finding would lead to an expected factor of about 20 of the convoy electron yields for Ni (45 MeV/u) and Ar (95 MeV/u). This is in fair agreement with the experimental data reported in fig. 3b, the observed ratios being at least about 100.

With electron-carrying (not fully stripped) projectiles such as $^{36}Ar^{17+}$ at 93 MeV/u [4] and even at energies as high as 390 MeV/u [15], convoy electrons are clearly observed and stem from electron loss to continuum (ELC). A weak CE component is also observed for fully stripped Ar at 35 MeV/u and for carbon targets [4].

In the present experiment with bare Ar ions, a most striking result is the lack of the convoy peak for the carbon target (fig. 1), at the most forward angles, down to $\approx 1.5°$, especially if compared to the case of a gold target of equal or even smaller thickness. This could be a manifestation for a "threshold" effect for convoy electron production at relativistic velocities, in agreement with the ECC data of Breinig *et al.* [3]. These data, obtained with He, Ne and Ar gas targets (shown in fig. 4) do also suggest such a threshold behavior: the ECC yield for He is two orders of magnitude lower than for Ne and Ar. If the convoy electron had followed a smooth evolution down to C, in continuation of the yield curves shown in fig. 4, we should have observed convoy electrons in view of the detection limit, in particular at 2°.

The following argument may explain these findings: For efficient capture to take place, a velocity matching of projectile and target electrons (*i.e.* the high-momentum wing of the Compton profile) is necessary. Possibly, such a matching is impossible for the carbon target, but becomes possible for strongly bound inner-shell electrons with the heavier targets.

4.3 Very fast electrons

Finally, we comment on two interesting features visible in the spectra of figs. 1 and 2. In the case of gold targets, a tail extending beyond the high-energy part of the BE peak is observed. Such electrons with velocities far beyond that of binary-encounter electrons are present for all the forward angles up to 60°. This can only in part be due to the Compton profile of the gold target, since only the most strongly bound inner-shell electrons have a sufficiently large Compton profile to allow ejection at high enough velocities. The contributions of electrons from different shells scale roughly with the inverse cube of the binding energy of the electrons, *i.e.* with E_B^{-3} [16]. The yield of high-energy electrons is several orders of magnitude too large to be explained by this contribution [8,10].

An additional mechanism consists in multiple collision sequences of electrons between target and projectile nuclei. This is often referred to as "Fermi shuttle" acceleration mechanism, since it was suggested by E. Fermi to explain high-energy cosmic rays [17]. Quite recently, convincing experimental evidence has been found for such a mechanism in ionizing ion-atom [18] and ion-solid [8, 10] collisions. In this acceleration scheme, a part of the BE electrons produced in the collision interacts with the target atoms along the ion trajectory. Possibly, they are scattered back with a certain velocity distribution, and a certain probability of colliding again with the same incident nucleus. We emphasize that the probability of such higher-order processes may be sharply enhanced in ion-solid collisions as compared to ion-atom collisions, because of the high target nucleus density. We made simple Monte-Carlo–type calculations (described in detail in [8, 10]), which reproduce in a satisfactory way the tails of the BE velocity spectra, thus giving strong evidence for such an acceleration scheme to take place.

As can be seen from fig. 2, high-energy electrons up to more than twice the projectile velocity are observed in the backward direction. For solid thick targets, an important part of the initially forward-emitted electrons further interact with the target atoms, so that a fraction of them are deviated and backscattered at large angles. This is the onset of the above-mentioned Fermi shuttle. We expect also that this effect should depend on the atomic number of the scattering center. Absolute values obtained at 130° (Ar) and at 140° (Ni) are shown in fig. 3c as a function of the target atomic number. A strong increase of the cross-section with target atomic number is observed. This is an evidence for the importance of the target atomic number of the scattering centers in the production of fast electrons at backward angles.

5 Conclusion

In conclusion, we have shown the complexity of the production mechanisms of fast electrons at high projectile velocities. The production cross-section for convoy electrons strongly depends on the target atomic number and on the beam energy. In particular, we do not observe convoy electrons in the case of a carbon target for a 95 MeV/u $^{36}Ar^{18+}$ beam, probably because of a velocity mismatch between projectile and the target electron Compton profile. The amount of "intermediate" electrons with velocities in between the beam velocity and two times the beam velocity, increases with the atomic number of the target (fig. 1). An ionization mechanism closely connected to the "Fermi shuttle" concept for the emission of such electrons with velocity larger than the projectile velocity was recently found in complex calculations of inner-shell ionization of collisions of heavy ions with heavy target atoms [19]. Further evidence for the "Fermi shuttle" acceleration was found for the heaviest target (Au), where an enhancement of the high-velocity tail in the BE peak is observed. This finding can be explained with a multiscattering mechanism, where electrons undergo multiple collision sequences between target and projectile. We have also observed that fast electrons are present also at backward angles, this process being the onset of the Fermi shuttle. Their production cross-section strongly increases with the target atomic number.

We compared absolute doubly differential cross-sections for binary-encounter electron ejection from C targets to a transport theory which is based on the relativistic electron impact approximation (EIA) for electron production and which accounts for angular deflection, energy loss, and energy straggling of the transmitted electrons. Peak shapes and absolute values of DDCS and the angular distribution of SDCS are well reproduced by theory (for more details see ref. [13]).

The present experiment is an example for fruitful interdisciplinary collaboration and shows the great interest in applying powerful detectors, developed initially for nuclear-physics experiments, to atomic-collision studies. Further measurements of absolute high-energy electron ejection cross-sections, in a wider projectile energy range, and with both heavier and lighter ions, are in progress. Such basic data for ionization in atomic collisions with solids are important for the understanding of ion-induced effects in condensed matter with applications in *e.g.* solid-state physics and radiation medicine.

We would like to thank the GANIL staff for providing the high-quality 95 MeV/u ^{36}Ar beams, N. Giudice, N. Guardone, V. Sparti and S. Urso (INFN Catania), J. Cacitti and R. Beunard (GANIL) for invaluable help during the mounting of the experiment, and C. Marchetta (LNS Catania) for target preparation. We thank Doris Jakubassa-Amundsen (Munich) for important discussions and calculations. This work has been supported by the European Community Access to Research Infrastructure Action of the Improving Human Potential Programme, contract No. HPRI-CT 1999-00019.

References

1. J. Frankland, H. Rothard, M. Bex (Editors), *Research at GANIL 1998-2000 - A Compilation* (Caen/France, 2002).
2. N. Stolterfoht, R.D. Dubois, R.D. Rivarola, *Electron Emission in Heavy-Ion-Atom Collision* Springer Ser. Atoms and Plasmas, Vol. **20** (1997).
3. M. Breinig *et al.*, Phys. Rev. A **25**, 3015 (1982).
4. B.D. DePaola, Y. Kanai, P. Richard, Y. Nakai, T. Kambara, T.M. Kojima, Y. Awaya, J. Phys. B **28**, 4283 (1995) and private communication.
5. T. Azuma, T. Ito, K. Komaki, T. Tonuma, M. Sano, A. Kitagawa, E. Takada, H. Tawara, Nucl. Instrum. Methods Phys. Res. B **132**, 245 (1997).
6. G. Lanzanò, E. De Filippo, S. Aiello, M. Geraci, A. Pagano, Sl. Cavallaro, F. Lo Piano, E.C. Pollacco, C. Volant, S. Vuillier, C. Beck, D. Mahboub, R. Nouicer, G. Politi, H. Rothard, D.H. Jakubassa-Amundsen, Phys. Rev. A **58**, 3634 (1998).
7. H. Rothard, D.H. Jakubassa-Amundsen, A. Billebaud, J. Phys. B **31**, 1563 (1998).
8. G. Lanzanò, E. De Filippo, D. Mahboub, H. Rothard, S. Aiello, A. Anzalone, S. Cavallaro, E. Geraci, M. Geraci, F. Giustolisi, A. Pagano, G. Politi, Phys. Rev. Lett. **83**, 4518 (1999).
9. D.H. Jakubaßa-Amundsen, H. Rothard, Phys. Rev. A **60**, 385 (1999).
10. G. Lanzanò, E. De Filippo, D. Mahboub, H. Rothard, S. Aiello, A. Anzalone, S. Cavallaro, E. Geraci, M. Geraci, F. Giustolisi, A. Pagano, G. Politi, Phys. Rev. A **63**, 032702 (2001).
11. H. Rothard, G. Lanzanò, D.H. Jakubaßa-Amundsen, E. De Filippo, D. Mahboub, J. Phys. B **34**, 3261 (2001).
12. D.H. Jakubaßa-Amundsen, J. Phys. B **30**, 365 (1997).
13. E. De Filippo, G. Lanzanò, H. Rothard, C. Volant, D.H. Jakubaßa-Amundsen, S. Aiello, A. Anzalone, N. Arena, M. Geraci, F. Giustolisi, A. Pagano, Phys. Rev A **68**, 024701 (2003).
14. P. Koschar *et al.*, in *Forward Electron Ejection in Ion Collision*, edited by K.O. Groeneveld, W. Meckbach, I.A. Sellin, Springer Lect. Notes Phys. LNP, Vol. **213** (1984) p. 129.
15. Y. Takabayashi, T. Ito, T. Azuma, K. Komaki, Y. Yamazaki, H. Tawara, M. Torikoshi, A. Kitagawa, E. Takada, T. Murakami, Phys. Scr. T **80**, 249 (1999).
16. G.N. Ogurtsov, Rev. Mod. Phys. **74**, 1 (1972).
17. E. Fermi, Phys. Rev. **75**, 1169 (1949).
18. B. Sulik, Cs. Koncz, K. Tőkési, A. Orbán, D. Berényi, Phys. Rev. Lett. **88**, 073201 (2002).
19. D.C. Ionescu, A. Belkacem, Eur. Phys. J. D **18**, 301 (2002).